Rev. Adv. Mater. Sci. 38 (2014) 160-175

A REVIEW ON THE FABRICATION AND PROPERTIES OF PLATINUM NANOPARTICLES

A.L. Stepanov[1,2,3], A.N. Golubev[2], S.I. Nikitin[2] and Y.N. Osin[2]

[1]Kazan Physical-Technical Institute, Russian Academy of Sciences, 420029 Kazan, Russian Federation
[2]Kazan Federal University, 420018 Kazan, Russian Federation
[3]Kazan National Research Technological University, 420015 Kazan, Russia

Received: January 26, 2014

Abstract. A review on chemical and physical preparation of platinum nanoparticles and some applications with these nanoparticles is presented. Application perspectives such fields as nanocatalysts, electrical conductivity, optics and nonlinear optics are demonstrated. Different parameters and condition of various fabrication technologies are considered and realized specific physical properties of platinum nanoparticles are discussed.

1. INTRODUCTION

The search for new functional materials is one of the defining characteristics of modern science and technology. Metal nanoparticles (MNPs), in particular, platinum nanoparticles (PtNs) can possess a wide range of properties that can be used for many practical applications. Nanostructured materials show much interdisciplinary effort. Both chemical and physical properties was found to be fruitful and, in many cases, fascinating in this nanosize range. MNPs are of interest due to their special properties in many aspects, such as catalysis and applications of optical devices.

Many physical and chemical properties of modern materials for electronics, optics, chemical reactions, and other high-tech applications depend closely on the manufacturing process. Synthesis and processing of MNPs pose a number of difficulties, especially in terms of reactivity and agglomeration. The remarkable reactivity of MNPs, which makes them potential candidates, for instance, as catalysts, is associated to their high fraction of surface atoms as compared to conventional bulk materials. In certain applications, a uniform dispersion of nanoparticles is required. MNPs usually present different characteristics from their corresponding bulk phase because of their finite size or equivalently the large fraction of atoms located near or at the particle surface, which can lead to significant changes in structural and chemical properties of the composite system.

Due to potential technological interests of PtNs, the synthesis and study of nanoparticles was a very active field of research during last years. Platinum-containing films could be used for enzyme immobilization, optical applications, and catalytic activity. For instance, the enhanced catalytic activity of PtNs plays an important role in the reduction of pollutant gases exhausted from automobiles [1,2]. In particularly, these studies of nanostructured materials show a strong dependence of their properties on size and shape. For example, the size effect on the catalytical efficiency is known, and the perspective effect on catalysis by the shapes of metal nanoparticles is anticipated and under investigation. Also the stability of PtNs is of great importance to the development of efficient and durable proton exchange membrane fuel cells [3,4] and the coalescence of PtNs is responsible for a reduction in the electrochemically active surface area that reduces cell perfor-

Corresponding author: A.L. Stepanov, e-mail: aanstep@gmail.com

mance [5]. Furthermore, PtNs is used widely in the electronics industry for the manufacture of conductive thick film circuits and internal electrodes of multilayer ceramic capacitors [6].

In the present review, recent advantages and some examples on PtNs preparation methods and some most critical application are reviewed and discussed in the frame of novel photocatalytic, electric, optical and magnetic nastructure materials with PtNs.

2. NANOPARTICLE SYNTHESIS METHODS

2.1. Chemical Preparation

Chemical preparation method means a synthesis of MNPs in chemical solution and quite often such MNPs called as colloid metal particles. In such case the main variations in chemical preparation of colloidal particles is going from the different chemical reactions and chemical compositions, which are used for this purposes. For instance, chemical reduction of metal ions inside reversed micelles in a nonpolar solvent is most commonly employed in the preparation of MNPs. A metal salt dissolved in water is confined inside the reversed micelles and is reduced into MNPs by chemical reduction. The diameters of the nanoparticles are controlled by the effective volumes of the reversed micelles, which are varied by changing the amount of water inside the reversed micelles with changing a molar ratio of water to the nonpolar solvent. Consider some key examples of chemical techniques used for synthesis of PtNs in various solutions.

2.1.1. Shape-controlled synthesis

Many studies on colloidal metal particles have focused on the control of particle sizes and their growth kinetic by polymeric stabilizers in solution. It was shown that the degree of polymerization and the concentration of the stabilized polymer influence the size distribution and stability of colloidal particles. On the other hand, shape control of MNPs is much more difficult to achieve. Therefore, the influence of particle shape on catalytic activity was not reported to date. However, authors of the work [7] describe a novel approach for synthesis of colloidal PtNs with controlled shapes and sizes by changing the ration of the concentration of the capping polymer material to the concentration of the cations Pt^{2+} in solution at room temperature. For that purpose the PtNs were prepared by the traditional known method [8, 9]. A solution of 1×10^{-4} M K_2PtCI_4 was prepared in 250 ml of water, to which we added 0.2 ml of 0.1 M sodium polyacrylate (sample 1). The spatial feature of this technique is an use of a bubbled gas through the solution during chemical reactions. The Pt ions were reduced by bubbling H_2 gas at a high flow rate through the solution. The reaction vessel was then sealed, and the solution was left overnight. After 12 hours colloidal PtNs were formed. Additional sample 2 was prepared by adding to the starting solution 1.0 of the 0.1 M polyacrylate solution, respectively, and following the same procedure. In the work [7] åhe initial ratios of the concentration of the capping material to that of the metal cation in the solution were selected to be 1:1 and 5:1 in samples 1 and 2, respectively.

As seen from TEM sample 1 predominately containing particles with a square outline (Fig. 1, left), whereas sample 2 contained high proportions of particles with a triangular outline (Fig. 1, right). By tilting the samples in the TEM, it was detected that square outline were found to be cubic, and those triangular outlines were tetrahedral. These shapes were also observed in some Pt colloids together with tetrahedral, polyhedral and irregular-prismatic particles in same solution [9,10].

2.1.2. Chemical reduction

An effective control of particle size continues to be the quite difficult challenge for researchers involved in the synthesis of colloidal metal dispersions. In addition, since individual nanoparticles have a tendency to form agglomerates during the preparation process, control of particle-particle interaction is critical for obtaining a stable dispersion. To ensure the preparation of individual MNPs, it is particularly important to inhibit the formation of hard agglomerates through a physical-chemical bond, or neck of MNPs with environment chemical components.

To solve such aggregation problem in the work [11] metallic dispersions of finely divided PtNs in ethylene glycol was prepared. This organic material serves both as solvent and reducing agent of metal species. Synthesis of these colloid metals was achieved by varying the reaction temperature, the initial concentration of metal compounds, and the character and order of addition of reactants. In more detail, 45 ml of ethylene glycol were heated up to 150 °C at a rate of 5 °C/min, then a 5 ml solution EG-H_2PtCl_6 (500 mg) are injected into the hot ethyeleneglycol and 25 ml poly(N-vinyl-2-Pyrrolidone) (PVP) solution of protective agent (100 mg or 500 mg) are added drop by drop with the aid of a peristaltic pump. The addition of PVP takes

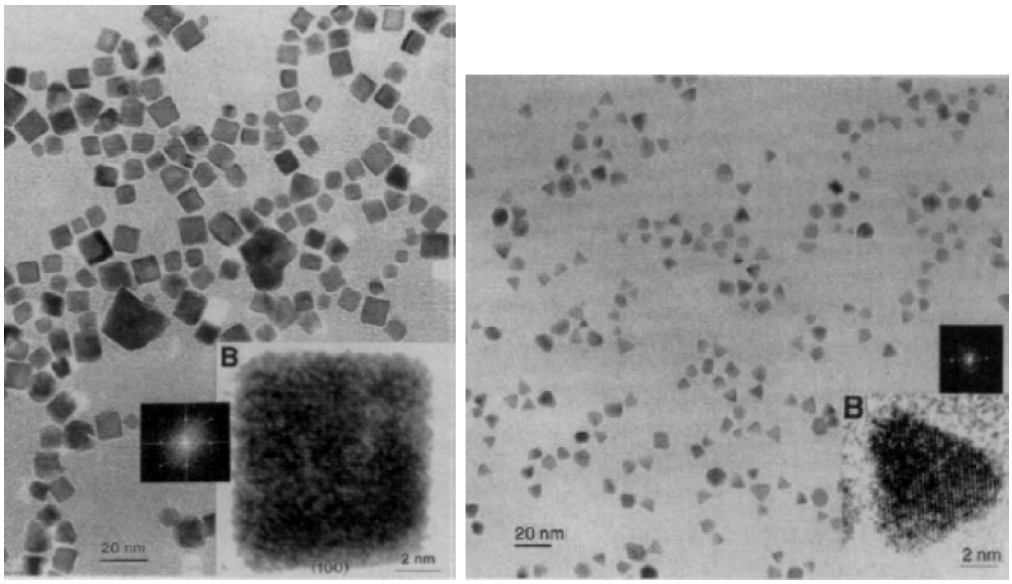

Fig. 1. TEM images of sample 1 (left) and sample 2 (right), indicating the cubic particles and the abundance of tetrahedral, respectively. Insets show high-resolution lattice images. Replotted from Ref. [7].

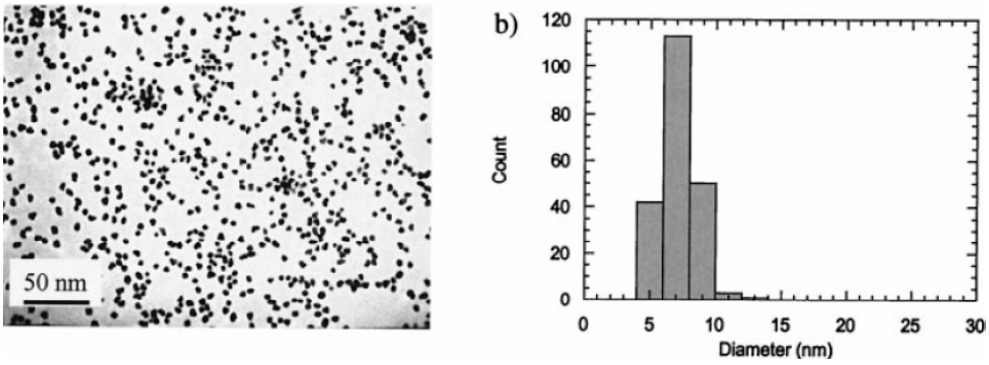

Fig. 2. Micrographs and the corresponding histograms of PtNs synthesized from hexachloro platinic acid in ethylene glycol in the presence of PVP (500 mg. c). Replotted from Ref. [11].

about 13 min, and then the reaction is stopped after one hour.

The hexachloroplatinic complex is stable towards reduction by ethylene glycol at room temperature, but it is reduced at 110 °C into elemental platinum. The product obtained after four hours of reaction was found to be composed of colloidal particles with a size smaller than 10 nm and with a considerable degree of sintering. To achieve colloidal platinum dispersions with a narrow size distribution and free of sintering, small amounts of PVP were required. Excess PVP (between 1 g and 3 g) inhibited completely the reduction of $PtCl_6^{2-}$ perhaps due to the formation of a stable complex. Regardless of the experimental conditions used, the size of platinum colloids obtained was always about 7 nm. Fig. 2 (left) shows TEM micrographs of colloidal platinum. The corresponding histogram is also presented in Fig. 2 (right). Even though the particle size distribution of colloidal platinum is very narrow, it exhibits no regular particle shape. X-ray powder diffraction of these nanoparticles revealed a well-crystallized Pt metal state.

2.1.3. Curing one-step process in polymer

The authors of the study [12] demonstrated a simple and inexpensive general process for the synthesis of PtNs embedded directly in polymer matrix, for example, in polydimethylsiloxane (PDMS). Such polymer was extensively used in applications that include microfluidic channels, lubricants, defoaming agents, gas separation membranes and catheters [13]. This method circumvents the need of using pre-formed nanoparticles and gives a volume dispersion of nanoparticles without requiring any external reducing or stabilizing agent. The process involves preparing a homogenous mixture of platinum salt, siloxane elastomer and the curing agent

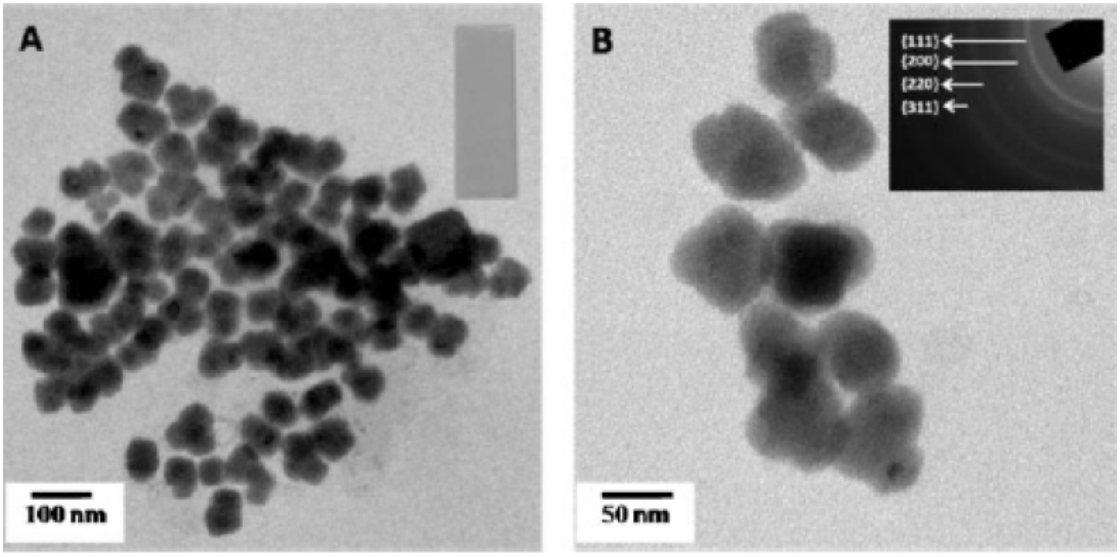

Fig. 3. TEM images of the PtNs in PDMS. Inset is the photograph of the diffraction PtNs pattern. Replotted from Ref. [12].

(hardener) followed by curing. During the curing process, the hardener performs a dual role of reducing the salt to form nanoparticles and cross-linking the elastomer. This in situ method avoids the use of any external reducing agent/stabilizing agent and leads to a quite good dispersion of nanoparticles in the polymer matrix. Nanoparticles act as filler and enhance the mechanical properties of PDMS. Young's modulus of nanoparticle containing film is three times higher than that of pure polymer film.

PtNs embedded PDMS film can be prepared by dissolving chloroplatinic acid using appropriate solvent and mixing with elastomer and hardener followed by curing [12]. TEM images of PtNs formed in PDMS are presented in Fig. 3. As seen, the nanoparticles are irregular and polydispersed in nature with an average particle size of 50 nm. The diffraction of platinum nanoparticles (inset of Fig. 3) indicates their fcc crystalline structure.

As was mentioned PtNs and polymers are usually synthesized separately and then mixed together to form the films [14]. In the work [15,16] the authors adopted in situ preparation method for making the Pt–PVA (Polyvinyl alcohol) films. High purity $H_2PtCl_6 \cdot 6H_2O$ and PVA (MW 13000–23000, 98% soluble) are taken at weight ratios ($H_2PtCl_6 \cdot 6H_2O$/PVA) of 0.003 and 0.006, respectively. PVA is dissolved in 25 ml of doubly distilled water, and H_2PtCl_6 is dissolved in 1 ml of doubly distilled water. Both solutions are mixed well and stirred for 30 min. The solutions are then kept in covered petri dishes, and allowed to dry in room temperature for 20 days. Pieces cut from the dried films are then annealed at 120 °C for 10 - 45 min, respectively. With higher annealing times the film color is found to change from light brown to dark brown. PVA acts as the reducing agent and stabilizer for the nanoparticles, and as the matrix for homogeneous distribution and immobilization. Thus an advantage of the present in situ preparation method is that PVA is the sole reducing agent, which reduces the $[PtCl_6]^{2-}$ and caps the PtNs. From the TEM it is seen that the particle size increases with the annealing time duration. Moreover, the nanoparticles seem to become more polygonal as the annealing time increases. Annealing at a higher temperature (180 °C) resulted in still bigger particles, and in the clusters seem to be sticking together to form a chainlike structure. Such chain formation has been discussed previously in the work [17], in the case of an unstabilized Pt colloid.

In the study [18] the polyol method was followed for the synthesis of the PtNs passivated with poly(N-vinyl-2-Pyrrolidone) (PVP). Hexachloroplatinic acid ($H_2PtCl_6 \cdot H_2O$) (99.99%), PVP (MW = 40 000) and 1,2-ethylenediol (99.95%) (EG) were used. For the synthesis of the PtNs, 0.4 g of PVP was dissolved in 50 mL of EG under vigorous stirring and refluxing at 413K. After temperature stabilization, 0.1 mM aqueous solution of the metal precursor was added to the EG-PVP solution with continuous agitation for 3 h under reflux. High-resolution transmission electron microscopy (HRTEM) and high angle annular dark field (HAADF) images are shown in Fig. 4.

2.2. Physical technique of nanoparticle preparation

There are a variety physical methods for preparation of MNPs in substrates or deposited on them.

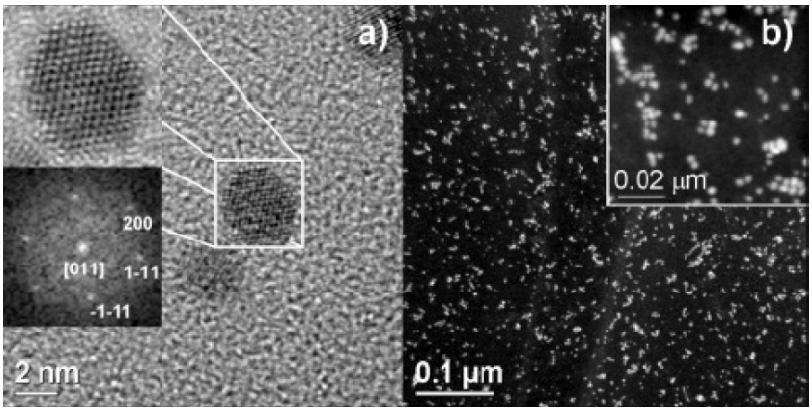

Fig. 4. (a) HRTEM image showing a truncated cuboctahedron PtNs. Upper inset shows a filtered image of the PtNs, indicating the separation between planes; the lower inset (diffractogram) reveals a (011) orientation of the nanoparticle, according to Ref. [19]. (b) HAADF images of the PtNs capped in PVP showing particles. Inset: at a higher magnification, the existence of islands in which the particles aggregation is apparent. Replotted from Ref. [18].

Here, examples most used in practice approached for fabrication of PtNs are observed.

2.2.1. Co-sputtering of platunum and matrix material and electron beam evaporation

By co-sputtering technique it was demonstrated that the composites of amorphous dielectrics matrix such as SiO_2 and Al_2O_3 with PtNs nanoparticles could be made [20]. In general, the concentration of Pt was monitored by depositing in each case the same number on the amorphous target of silica or alumina. The substrate was rotated during the deposition to ensure the homogeneity of the composites.

Additionally, it was developed a low electrical power, low pressure tilted target room temperature sputtering process to achieve uniformly distributed spherical PtNs of different sizes with high particle density and controllable inter-particle distance [21-23]. Varying the deposition time and RF power, while keeping the pressure and gas flow rate fixed controls the average size of these particles. Due to their unique tilted target deposition [21-23], these particles exhibit near homogeneous size distribution with good control of size and density. PtNs embedded a metal-oxide-semiconductor (MOS) structures were fabricated by depositing e-beam grown Al_2O_3 layer on low-doped (100) p-Si. Samples were then transferred to the sputtering system to deposit PtNs onto this layer. The deposition time was varied at 10, 20, and 30 s with 30 W RF power under 4 mTorr pressure and 10 sccm Ar gas flow at room temperature. Subsequent in situ H_2 annealing at 260 °C for 45 min was carried out. Fig. 5 shows the plane view TEM images of uniformly distributed 1.08 nm PtNs, where the density of the PtNs was found to be $6.6 \cdot 10^{12}$ cm^{-2}. The high resolution TEM (HRTEM) image in the inset of figure shows the mono-crystalline structure of PtNs deposited on the amorphous Al_2O_3 film.

In the work [24], thermal annealing of very thin layer with PtNs created by electron beam evaporation and buried in a capping ceramic material (SiO_2) towards controlled synthesis of metallic nanocrystals was suggested as a method for nanocomposite preparation. PtNs layers with three different thicknesses were deposited from 5 to 25 Å. A SiO_2 layer with thickness of 150 Å separated the Pt layer from the substrate, and a SiO_2 layer with thickness of 50

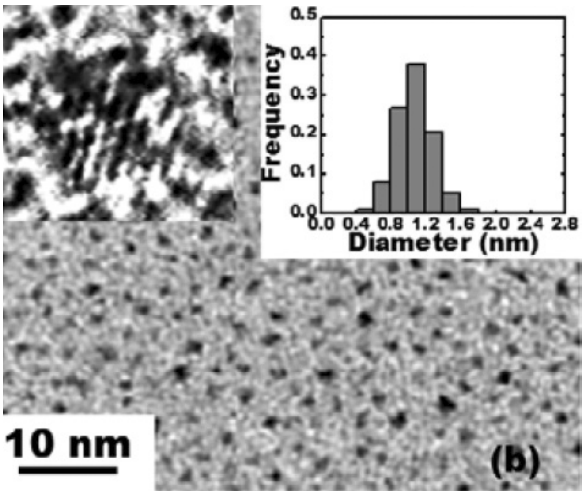

Fig. 5. Plane view TEM image of PtNs. Insets shows particle size distribution and HRTEM image. Replotted from Ref. [23].

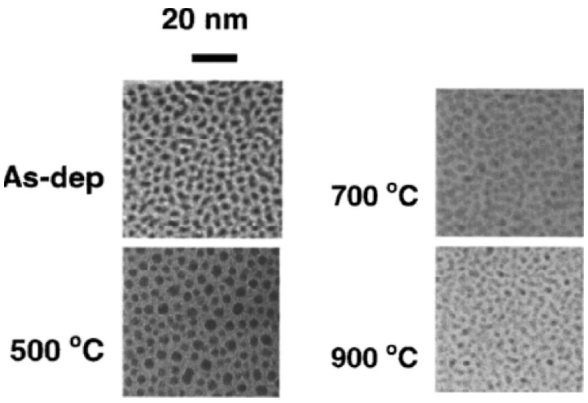

Fig. 6. TEM images of as-deposited PtNs with 5 Å thickness and after annealing 45º min at various temperatures, as indicated. Replotted from Ref. [24].

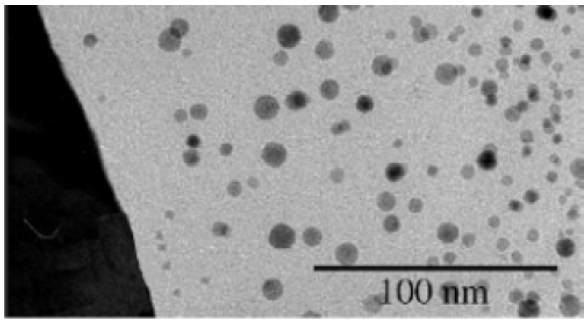

Fig. 7. TEM cross-section image of sample implanted with Pt ions and annealed at 1100 °C. Replotted from Ref. [29].

Å was deposited on the top. Deposition of these films was achieved by employing low deposition rates in the range of 0.5–2 Å/s. In Fig. 6 an example of deposited PtNs films is presented after laser annealing. Nanocrystal size can be controlled by tuning the thickness of the metallic layer and the annealing conditions. A relatively narrow size distribution was observed, with best results being obtained in samples with thinner PtNs layers (5 and 10 Å). In addition to size control, depth control can be naturally achieved by changing the thickness of the SiO_2 layers.

2.2.2. Ion implantation

Ion implantation offers a relatively simple and flexible means of fabricating MNPs in different host materials [25-28] and is therefore a useful tool for exploring such systems. The main advantages of using ion implantation are that concentration and depth distribution of implanted ions can easily be controlled accurately. Size distribution of nanoparticles can also be controlled to some extent with suitable implantation dose and annealing temperature.

Ion implantation can be also used for fabrication of PtNs in SiO_2 matrix [29,30]. For such purpose SiO_2 film thermally grown on Si substrate was implanted by Pt ions with high energy between 3.4 and 5.6 MeV and a dose range of $2\text{-}30\times10^{16}$ ion/cm^2 at liquid nitrogen temperature of irradiated substrate and followed by thermal annealing during one hour at temperature 1100-1300 °C [29,31]. TEM analysis revealed that the PtNs are spherical in shape (Fig. 7). The mean size of the PtNs varied between 2.8 and 3.6 nm for the highest and lowest ion energy, respectively, as determined with both TEM and X-ray scattering. Diffraction patterns obtained from the PtNs containing SiO_2 layer confirm that the nanoparticles have the bulk face-centered cubic (fcc) structure. The formation of PtNs for such compos-

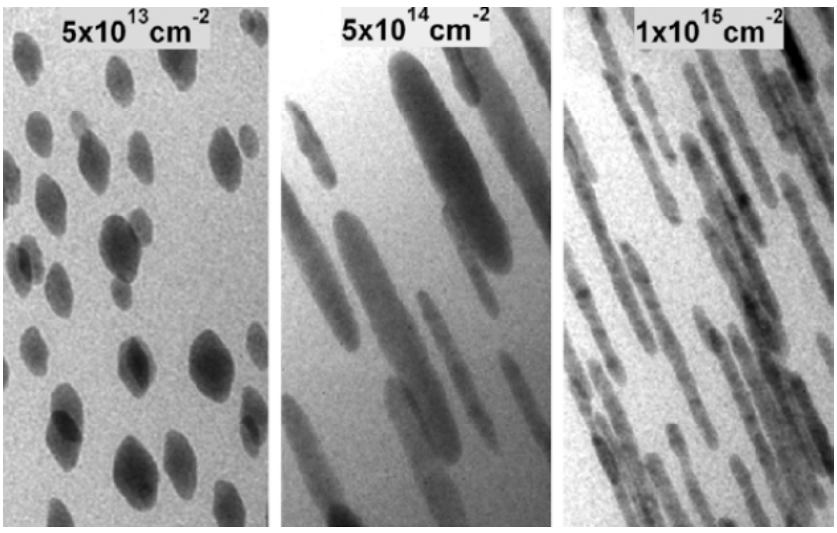

Fig. 8. TEM cross-section image of SiO_2 with implanted PtNs and irradiated with Au ions at 27 MeV. Replotted from Ref. [31].

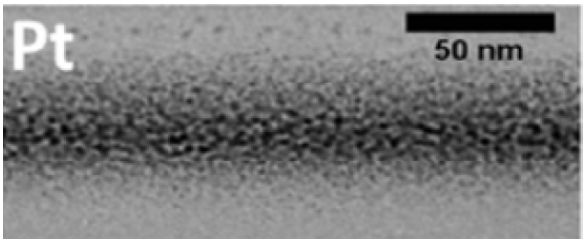

Fig. 9. TEM cross-section image of sample implanted with Pt ions and annealed at 900 °C. Replotted from Ref. [30].

ites was also determined by small-angle X-ray scattering (SAXS)] [32].

Subsequently, samples can be irradiated with 10, 15, 22, 27, 54, 89 or 185 MeV Au ions at room temperature with doses varying from $2 \cdot 10^{12}$ to $1 \cdot 10^{15}$ ion/cm^2 [31]. As example of such swift heavy ion irradiation, Fig. 8 shows TEM micrographs of samples irradiated with 27 MeV Au ions at different doses. As shown for embedded PtNs [31, 33, 34], swift heavy ion irradiation causes shape changes from spheres to prolate spheroids to rods aligned with the ion beam direction.

Low energy ion implantation (100 keV) and a dose 6'"10^{16} ion/cm^2 at room temperature can be also used for PtNs formation [30]. After implantation samples were annealed at 900 ºC in a nitrogen atmosphere for one hour. Fig. 9 shows cross-sectional image for implanted sample. Formation of PtNs is evident for this figure. The average size of PtNs is 1.6 nm, close to resolution limit of the TEM analysis. X-ray diffraction spectra consist of peaks at 39.8º, 67.5º, and 81.3º, which is corresponds to a single fcc Pt phase.

In the work [35] author demonstrated a possibility for synthesis of PtNs in polymer matrix - polymethylmethacrylate (PMMA) by very low energy (67 eV). PMMA is an important polymer because of its wide use as an electroresist for high resolution lithography. Thus, modification of this polymer to form a thin layer of metal-insulator composite may have important applications for micro- or nano-fabrication of devices. Ion implantation was performed using a filtered vacuum arc plasma system. A dense platinum plasma is formed by a compact vacuum arc plasma gun and transported through a magnetic filter to remove solid particulate contamination (macroparticles); the PMMA substrate is located several cm from the filter exit and is bombarded by the Pt plasma at the low energy of 67 eV; (subplantation is the term often used for this kind of very low energy ion implantation). A TEM image of the PtNs-PMMA composite is shown in Fig. 10, where the implanted dose was $0.4 \cdot 10^{16}$ ion/cm^2, corresponding to a composite below the percolation threshold. As seen composite material has an inhomogeneous nanoparticle size distribution.

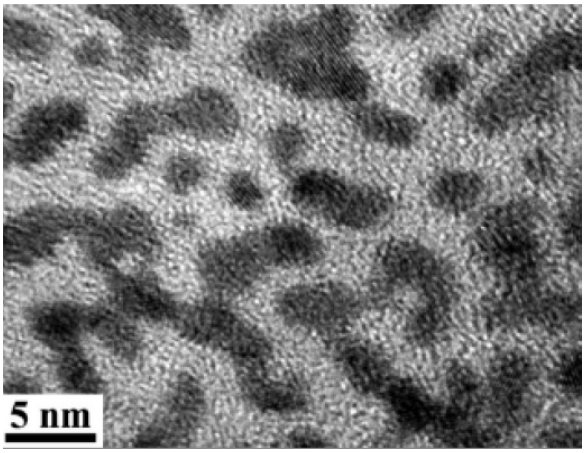

Fig. 10. TEM image of PMMA implanted with Pt-ions. Replotted from Ref. [35].

2.2.3. Ion implantation combained with surface etching

A nanoparticle fabrication technique, which combines high-energy ion implantation and surface etching, was firstly developed in the work [36] for catalyst applications. In this method, the seeds of nanoparticles are preserved inside the substrate by ion implantation and can be fabricated into nanoparticles by etching (Fig. 11). There are several advantages due to ion implantation, such as purity of the implanted ions and selection of a specific area for fabrication by controlling the quantity of ions by adjusting the ion dose and ion species. Using ion implantation with a dose of 3'"10^{16} ion/cm^2 and an energy of 3.1 MeV into (100) silicon substrate cooled to 95K following with etching the silicone surface during time from 10 to 30 min with 7.5 mol/l potassium hydroxide solution at 333K, PtNs were successfully fabricated [37]. Fig. 12 shows a SEM image of the substrate surface. Large cubic particles and small PtNs in environment were evident. The cubic particles uniform in size, about 80 nm and PtNs in background have a size between 5 and 20 nm.

2.2.4. Laser ablation in solution

The laser ablation of metal plates in solution such as, for example, sodium dodecylsulfate (SDS), was suggested as one of effective method for synthesis of MNPs [38,39]. Preparation of PtNs in solution of

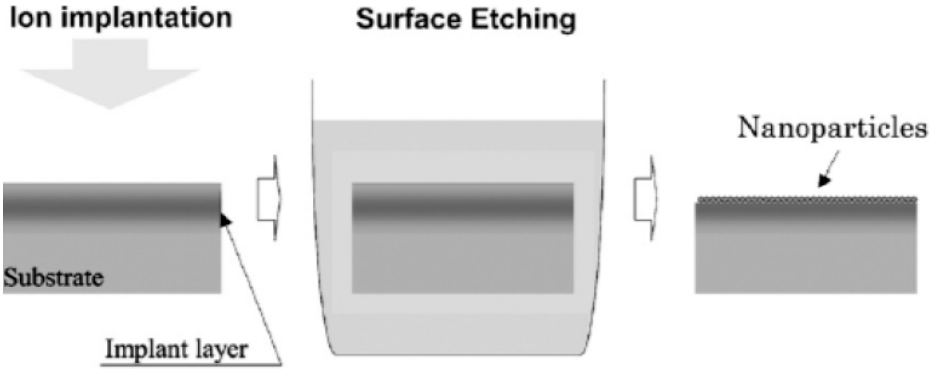

Fig. 11. Schematic of combined ion implantation and surface etching for fabrication of PtNs. First, ion implantation creates a layer of distributed Pt ions in a silicon substrate. Then, the silicon is etched, thus extracting PtNs. Replotted from Ref. [37].

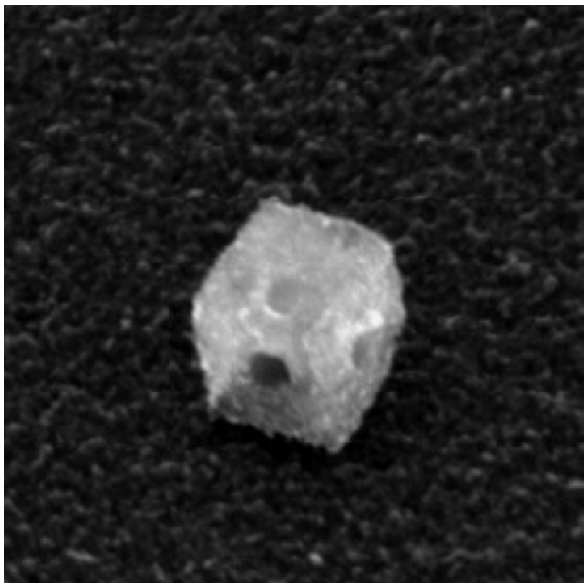

Fig. 12. Typical SEM image of a large cubic particle PtNs (background) after etching. Replotted from Ref. [37].

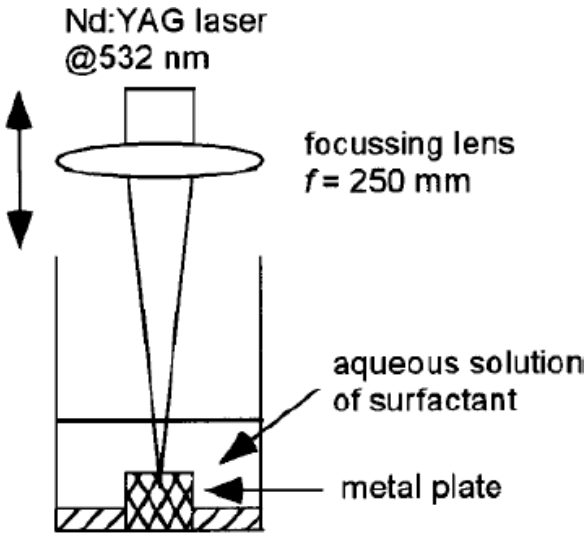

Fig. 13. Schematic diagram of the experimental apparatus. Replotted from Ref. [38].

SDS and in the pure water by same technique was realized also in the work [40]. For such aim the Pt plate or foil (> 99.99 %) was placed on the bottom of a glass vessel filled with an aqueous solution of SDS and of pure water. The metal plate was irradiated with a focused output of the fundamental (1064 nm) or second harmonic (532 nm) of Nd:YAG laser operating at 10 Hz with a lens having the focal length of 250 mm (Fig. 13) [38]. The spot diameter of the laser beam on the surface of the metal plate was varied (1.5-2 mm) by changing the distance between the lens and the metal surface. Upon irradiation of the laser beam, the solution was gradually turned into brown.

Fig. 14 shows typical TEM micrographs of PTNs produced by laser ablation (532 nm) of a platinum plate immersed in pure water. The average nanoparticle diameter produced in pure water is about 6.2 nm. Fig. 15 shows the average diameter of the PtNs as a function of the SDS concentration. As the SDS concentration increases, the average diameter remains unchanged up to the SDS concentration of 10^{-3} M and then decreases sharply.

3. PHYSICAL PROPERTIES AND APPLICATIONS

3.1. Optical properties

Nanometer-sized particles of free electron metals, such as Ag, Au, Cu, and Pt display interesting and useful optical properties. Their linear optical response is dominated by the surface plasmon resonance associated with the collective oscillation of the particles' free electrons [41]. Early, to demonstrate experimental extinction spectrum of PtNs in visible area and to compare this spectrum with another noble metal nanoparticles, various simplest MNPs suspensions in water were prepared in similar conditions [42]. As seen from Fig. 16, the mea-

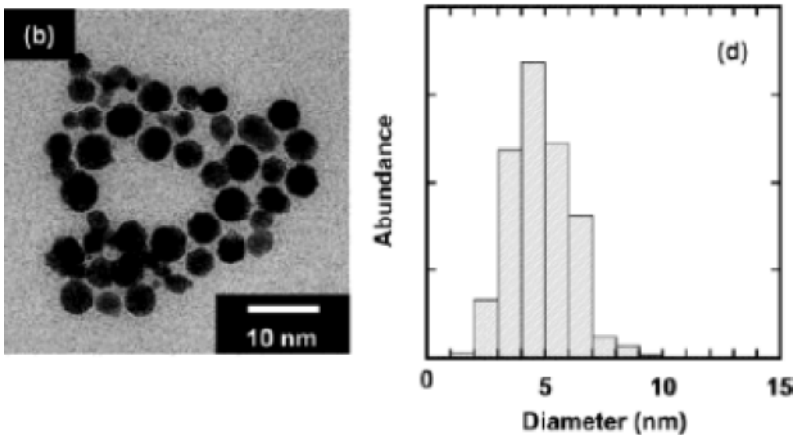

Fig. 14. TEM image of PtNs produced by laser ablation in pure water and a size distribution of nanoparticles. Replotted from Ref. [40].

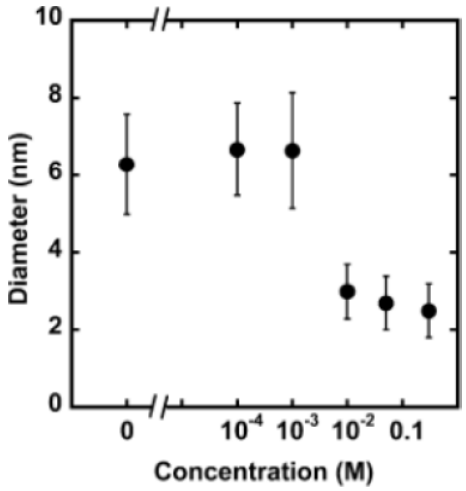

Fig. 15. Average diameter of PtNs produced by laser ablation (532 nm, 1.6 J/pulse cm^2) as a function of concentration of SDS in an aqueous solution. Replotted from Ref. [40].

sured extinction spectra for Ag, Au, and Cu exhibit typical plasmon absorption bands with maxima at 410, 520, and 564 nm, respectively. On the other hand, PtNs yield a featureless spectrum. In same time, the optical absorption spectra of an aqueous SDS solution, in which a platinum metal plate is ablated by a pulsed YAG laser [40], agree with a solution containing PtNs prepared chemically reasonably well [42].

An optical absorption of particles in a solution with smaller diameters than the wavelength of an incoming light (<500 nm) is given by the Mie theory [43], where the dielectric function of MNPs is written as a combination of an interband term and a Drude term for the conduction electrons in the particles [41]. The Mie theory was used for modeling of

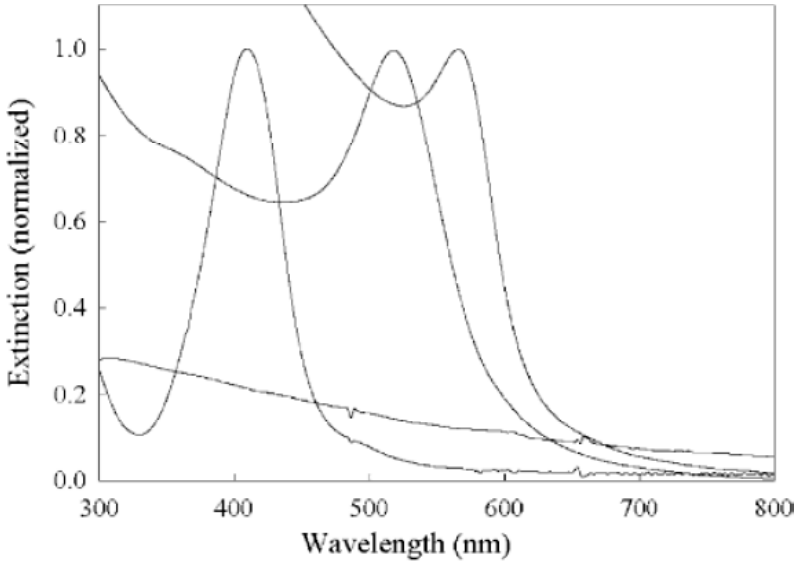

Fig. 16. Experimental extinction spectra of water solutions of the MNPs. The spectra with sharp surface plasmon absorption peaks are, from left to right, silver, gold, and copper nanoparticles. The featureless spectrum is of PtNs. Replotted from Ref. [42].

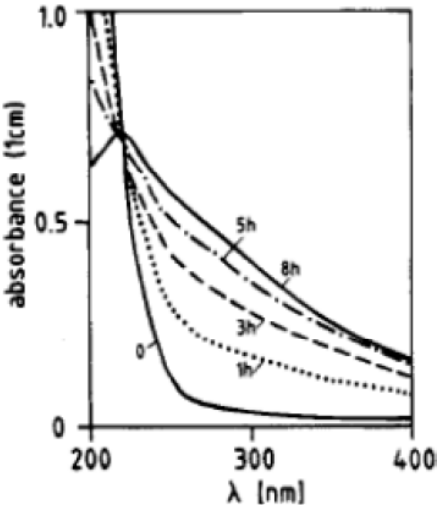

Fig. 17. Experimental extinction spectra of solutions with PtNs. Replotted from Ref. [9].

PtNs extinction when a size of nanoparticle was about 10 nm [42]. The resonance condition for PtNs was satisfied only for wavelengths to the blue of those considered in Fig. 16 (i.e., at 275 nm), and since imaginary part of dielectric constant $Im(\varepsilon_{Pt})$ is especially large for platinum, the resonance is extremely broad and hardly distinguishable.

Similar calculation of the optical absorption of PtNs based on the Mie theory showed that a plasmon peak appears at 215 nm [44]. Experimentally, it was demonstrated that a peak realy exists around 215 nm in the optical absorption spectrum of PtNs prepared chemically in solution (Fig. 17) and that the spectrum is almost independent of the particle size, although the absorption coefficient at the maximum was about 30% higher than the calculated one [9]. However, PtNs prepared by citrate reduction do not show any maximum around 215 nm, and the plasmon oscillation very slightly contributes to the total absorption. Nevertheless, previous experimental reports and theoretical calculation conclude that the surface plasmon absorption of PtNs should occur in the ultraviolet region [45-49].

3.2. Nonlinear optical properties

Optical limiters in the visible domain with a broad nonlinear optical spectrum and short response time are required for eye protection and switching applications. Study of optical properties of materials with ideal optical limiting performances has attracted substantial attention. With such aim an optical limiting performance of PVP-stabilized PtNs in methanol was analyzed with 8 ns pulses from a frequency doubled, Q-switched Nd:YAG laser at 532 nm [50]. The average size of PtNs was estimated by TEM to be of the order of 2 nm. As result Fig. 18 gives the optical limiting experimental dependence of PtNs-PVP. The transmitted energy shows a clamped curve as the input energy increases. The highest input energy was estimated to be of 3.5 mJ here used. It was found that the nonlinear transmittance decreases to 6.0%. Namely, it gives near 10 times attenuation in the incident energy.

The main nonlinear optical process responsible for strong optical limiting effect can be attributed to interband transition of platinum during the excitation of nanosecond pulses [51]. The contributions

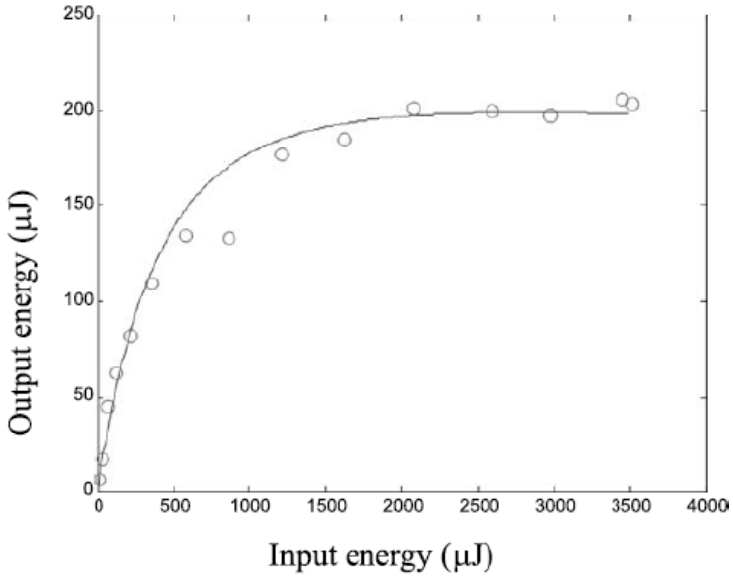

Fig. 18. The theoretical and experimental optical limiting results of PtNs-PVP in methanol with a linear transmission of 59% measured at the wavelength of 532 nm. Replotted from Ref. [50].

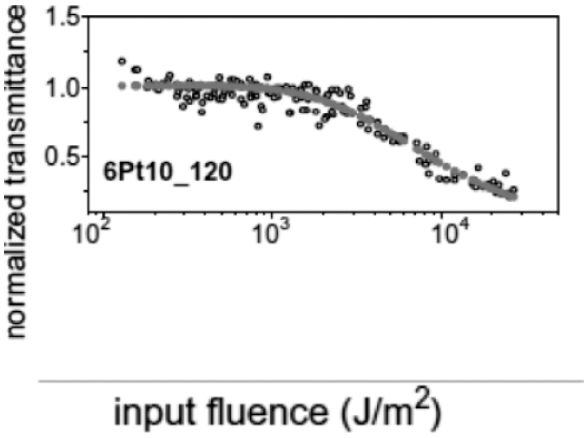

Fig. 19. Ultrafast nonlinear light transmission behavior of PtNs-PVA films. Circles are experimental data points, and the solid line is numerical fit. Replotted from Ref. [16].

of the interband transition to optical nonlinearities come from the photoexcitation of electrons out of the d band near the *X*-point of the Brillouin zone to the *s*–*p*-conduction-band states near the Fermi energy [51,52]. The electrons excited in an interband transition of platinum are free carriers possessing a whole spectrum of energies, both kinetic and potential, immediately after the absorption. The potential energies are those of the formerly unoccupied and occupied states within the conduction band. The excitation leads to the reduction in incident laser pulse energies.

In another work [16] free-standing platinum–polyvinyl alcohol nanocomposite (PtNs-PVA) films have been prepared. By thermal annealing of such samples, PtNs of different sizes and shapes have been obtained. Their optical nonlinearity was measured using ultrafast (100 fs) laser pulses at 404 nm, in the absorption wing region of the composites. A frequency-doubled Ti:Sapphire laser was used. The nonlinear transmission measurements were done in an open-aperture z-scan [52] configuration. In the z-scan experiment the input intensity can be varied in a smooth and continuous fashion. The laser pulse repetition rate was 1 Hz and laser energy densities was in the range of $1 \cdot 10^2$ to $3 \cdot 10^4$ J/m^2. Fig. 19 shows the typical nonlinear light transmission behavior extracted from the *z*-scan, where the normalized transmittance is plotted against the input laser fluency. The samples show a predominant optical power limiting behavior. As was concluded in the work [16] this nonlinearity is caused by the transient absorption of free carriers in the conduction band, which are generated in the primary absorption [16] which is possible originates from interband electron transitions.

In early study it was found significant absorption saturation in an aqueous solution of PtNs–PVP [53], but only induced absorption in an alcohol solution of Pt–PVP [50]. In both papers nanosecond laser pulses at 532 nm wavelength for excitation were used which is farther out in the absorption wing region. For bigger clusters (annealed at 180 °C) an absorption saturation was observed. As discussed above, both the observed absorption saturation and induced absorption are ultrafast processes, occurring within a 100 fs time window.

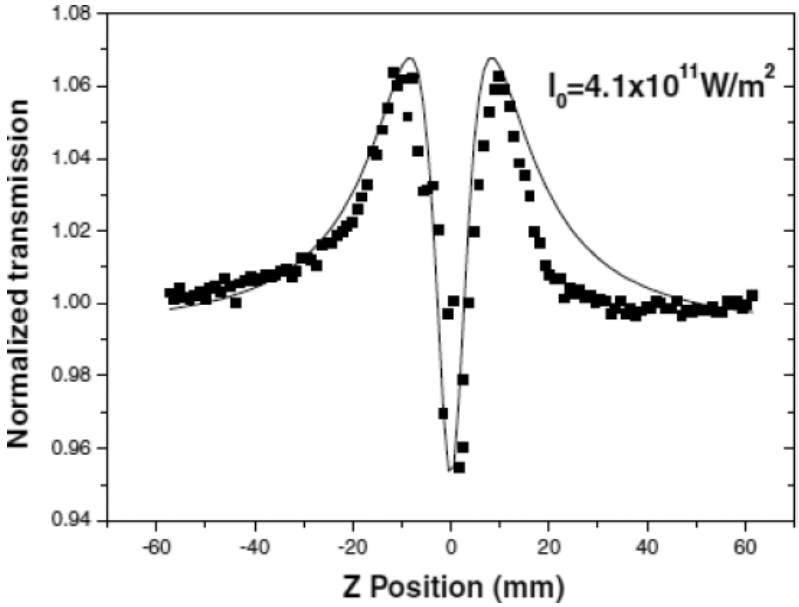

Fig. 20. Normalized transmission as a function of sample (PtNs–PVP) position for open aperture *Z*-scan. Replotted from Ref. [53].

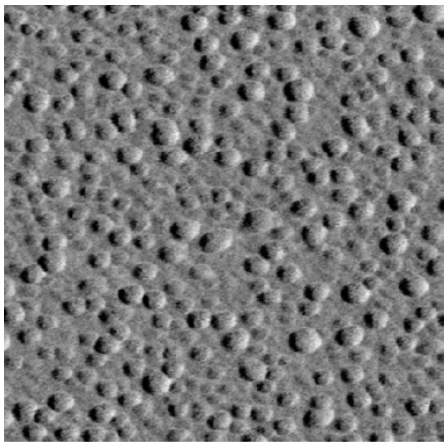

Fig. 21. The AFM image of deposited PtNs onto polystyrene surface. Replotted from Ref. [61].

Authors of the work [53] detected a shift from saturable absorption to reverse saturable absorption was observed at higher input pump intensities using open aperture *Z*-scan method. The transition process was analyzed using a phenomenological model based on nonlinear absorption coefficient and saturation intensity. The average size of PtNs–PVP was estimated by transmission electron microscopy (TEM) to be of the order of 2 nm. As example, the normalized transmittance of composite presented in Fig. 20. As seen, there are two composite nonlinear absorptions with opposite signs. This is because the nonlinear absorption of the sample transforms transforms from saturable absorption to reverse saturable absorption as the sample approaches focal point.

The nonlinear optical susceptibility of colloidal solution of metallic platinum was determined from the third harmonic generation measurements [54-56]. The dependence of the third harmonic intensity on the fundamental radiation intensity $I_{3\omega}(I)$ was measured using the Nd:YAG laser (λ = 1064 nm, t = 35 ps). The nonlinear susceptibility of colloidal platinum $\chi^{(3)}(-3\omega; \omega, \omega, \omega)$ was estimated to be $1.5 \cdot 10^{-14}$ esu. The nonlinear refractive and nonlinear absorption coefficient of suspensions with PtNs using the 729 nm femtosecond end picosecond pulses were done in the works [57,58]. The PtNs suspension showed a weak refractive nonlinearity, while it demonstrated a strong saturated absorption dominated over the positive nonlinear refraction in the closed aperture *Z* scans. The saturated absorption was observed both in the cases of 210 ps and 120 fs probe pulses. The change from saturated absorption to reverse saturated absorption in PtNs suspension was detected at the high intensities of 120 fs pulses.

3.3. Cataliysis

PtNs were especially studied in the field of catalysis because of their important industrial applications, including the reduction of pollutant gases from automobiles [59]. PtNs have shown catalytic reactivity highly dependent on particle morphology and the importance of a detailed understanding of these systems [60]. One of the most important problems, whose solution is needed for many practical applications of metal nanoparticles, is the formation and attachment of “two dimensional” nanoparticle ensembles on various planar substrates. Successful preparation of such-type composites is a promising way of creating peculiar “chips,” which can be used as convenient and inexpensive active elements of catalytic reactors, various sensors, etc.

As example, it is possible to consider catalytic properties of PtNs deposited onto polystyrene surface from a colloidal hydrosol solution [61]. During the adsorption on polymer substrate, PtNs form rather densely packed ordered monolayer ensembles with high catalytic activity in the model reaction of hydrogen reduction of methyl viologen (dimethyl-4,4'-bipyridine) in aqueous alkaline solutions [62]. The synthesized platinum particles have a spherical shape, their sizes fit the 5–8 nm range, and their average diameter is of approximately 7 nm. The AFM experiments demonstrated that PtNs form ordered “two-dimensional” structure on polystyrene surface (Fig. 21).

The reaction between hydrogen and methyl viologen catalyzed by PtNs was conducted in a special small all-glass vessel equipped with additional “finger” with quartz optical cell at the end. The procedure was as follows [62]. Water (4 ml) was poured into the vessel, and silicon wafer coated with polystyrene with deposited PtNs was immersed into water. After degassing, 0.1 M NaOH (0.5 ml) and $1 \cdot 10^{-2}$ M methyl viologen (0.5 ml) solutions were added to the system followed by filling with hydrogen under the pressure of 1 atm. The optical absorption spectra were recorded on a UV/VIS-Specord spectrophotometer at continuous stirring of solution. The kinetics of methyl viologen reduction was measured by recording an increase (with time) in the intensity of the absorption band of radical-cation [63].

The hydrogen reduction of the methyl viologen ion (MV^{2+}) in aqueous alkaline solution catalyzed by colloidal platinum can be described by the following overall equation:

$$2MV^{2+} + H_2 \Rightarrow 2MV^{+} + 2H^{+}. \quad (1)$$

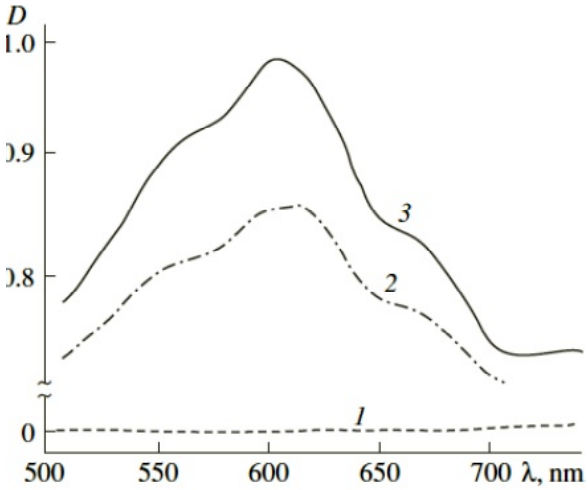

Fig. 22. Absorption spectra of aqueous solution containing methyl viologen and NaOH in the presence of Si/polystyrene plate with deposited PtNs: (1) in the absence of hydrogen, (2), and (3) 60 and 120 s after cell filling with H_2, respectively. Replotted from Ref. [61].

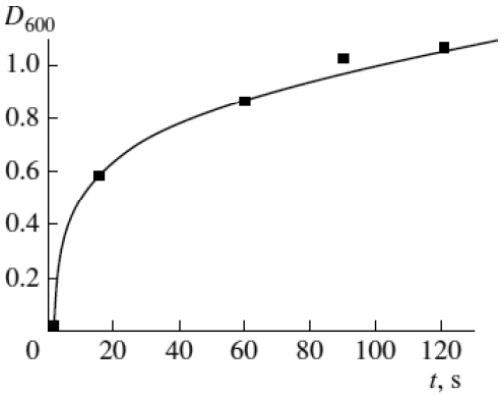

Fig. 23. Time dependence the absorption of radical-cations in solution in the presence of Si/ polystyrene plate with deposited PtNs after cell filling with hydrogen. Repotted from Ref. [61].

In the presence of the Si/polystyrene plate with deposited colloidal platinum in the aqueous methyl viologen solution, the formation of the reduction product (radical-cation) is observed immediately after filling the vessel with molecular hydrogen. These radicals are identified by the appearance of characteristic absorption with maximum at 600 nm and shoulders at 580, 660, and 730 nm (Fig. 22). The reaction proceeds in time (Fig. 23) and tends to achieve the state of complete reduction of methyl viologen ions that are present in the solution.

3.4. Conductivity

Rapid improvement in recent years of the performance of zinc oxide (ZnO) in transparent conducting oxides has distinguished ZnO as a promising material alternative to indium tin oxide (ITO). There are many characteristics of ZnO that may enable its efficient utilization in various novel devices. ZnO is an n-type semiconductor with a wide band gap of 3.37 eV. It has therefore been considered promising for use in the development of light-emitting structures and solar cells. But, due to the low conductivity of ZnO compared to metal and ITO, doping and hybridization with metal nanoparticles have been sujested [64] For such purposes PtNs can also applied.

PtNs using a methanol reduction method were synthesized and incorporated 0.25 at.% PtNs in order to enhance the electrical properties of the ZnO films while maintaining good transmittance for application in transparent conducting oxides [6]. A direct-patterning process using a photosensitive stabilizer and UV light was carried out. Fig. 24 displays an optical image of a direct-patterned ZnO hybrid film containing PtNs.

The sheet resistance of the ZnO films, both with and without PtNs, is shown in Fig. 25 as a function of annealing temperature. The values for ZnO films without PtNs annealed at 500, 600, and 700 °C were 0.572, 1.628, and 2.150 MW/cm, respectively, and the values for ZnO films with PtNs were 0.098, 0.221, and 0.674 MW/cm, respectively. These results are comparable to the reported values for ZnO film, for example, 1–10 MW/cm [65]. In this case, both types of ZnO films annealed at 500 °C showed minimum sheet resistance values. The ZnO films with PtNs showed reduced sheet resistance values due to an effective increase in the average carrier concentration. With similar approach a conductivity of the composite system based on SnO_2 films with PtNs were also studied [66].

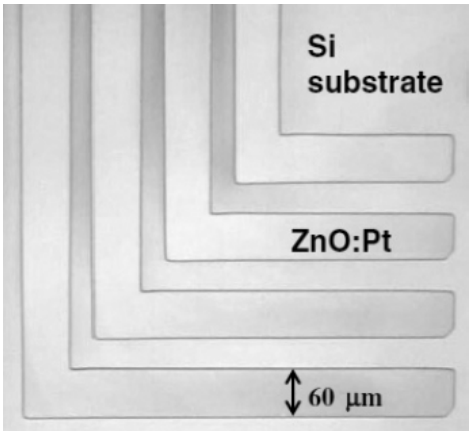

Fig. 24. Optical image of direct-patterned ZnO film with PtNs after annealing at 500 °C for 1 h. Repotted from Ref. [6].

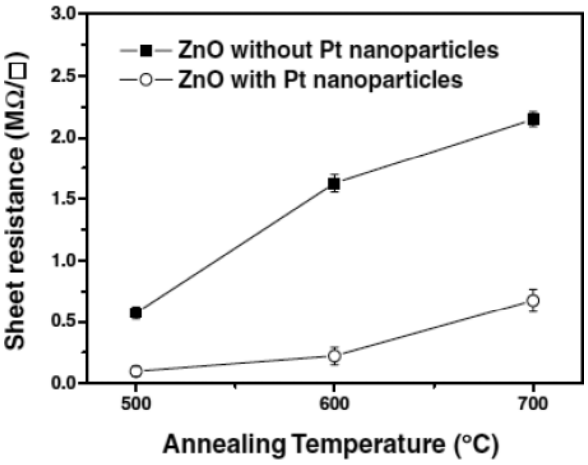

Fig. 25. Sheet resistance of ZnO films with or without PtNs at various annealing temperatures. Replotted from Ref. [6].

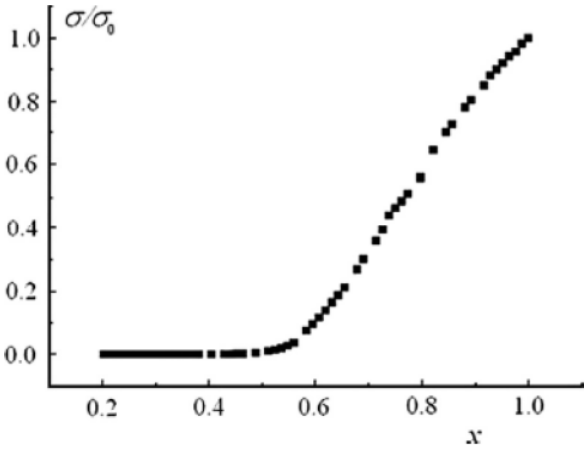

Fig. 26. Conductivity ratio σ/σ_0 as a function of the normalized platinum concentration x. Replotted from Ref. [35].

The transition from insulating to conducting phase was explored for PMMA with ion-synthesised PtNs [35]. In situ resistivity measurements were performed as the ion implantation proceeded. The electrical conductivity, σ, of composites with MNPs, near the critical transition where the material changes from insulator to conductor, can be described by a power law [67], $\sigma \cong \sigma_0(x - x_c)^t$; where σ_0 is a proportionality constant; x is the normalized platinum atom concentration of the conducting phase; x_c is the critical concentration, or percolation threshold, below which the composite has zero conductivity; and t is the critical exponent factor. The value x is the ion implantation dose ratio $\varphi = \varphi_0$, where φ_0 is the maximum dose for which the metal/polymer system remains a conductor/insulator; for doses greater than φ_0 ($x = \varphi/\varphi_0 > 1$), a metal film starts to be deposited on the polymer surface and the sample begins to take on the characteristics of a thin metal film. The measured conductivity ratio σ/σ_0 as a function of the normalized platinum concentration x is shown in Fig. 26, where φ_0 is the maximum dose for which the PtNs-PMMA system remains an insulator/conductor composite. As shown in [35], the maximum dose value φ_0 is $1.6 \cdot 10^{16}$ ion/cm^2.

3.5. SINGLE ELECTRON TUNNELING

Single electron devices utilizing the Coulomb blockade effect are promising candidates for future ultra-high density and ultra-low power integrated circuits. Room temperature observation of the single electron tunneling (SET) phenomenon requires that the self-capacitance and size of the island must be sufficiently small such that the Coulomb charging energy is much larger than the thermal energy. Evidence of size dependent SET behavior from *I–V* characteristics of the sub-2 nm PtNs embedded MOS structure was reported [23]. Notably different amounts of electron addition energy and SET peaks with different heights were observed with size tunable PtNs. This strongly supports nanoparticle fabrication as a potential step in current CMOS processing for incorporating future SET applications.

In the work [23] the *I–V* measurements for Al_2O_3 layer with PtNs were performed in the dark at room temperature. As example, Fig. 27 shows the *I–V* characteristics of the MOS structure under positive bias for with embedded PtNs of size 1.08 nm. It is shown that specific tunneling characteristics such as distinct tunneling current peaks were observed

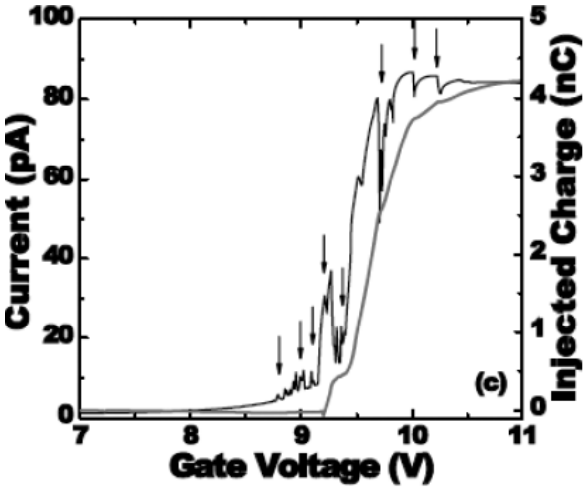

Fig. 27. *I–V* characteristics of 1.08 nm size of PtNs embedded MOS structure at room temperature. The arrow indicates the onset of an abrupt increase of current jump in each peak. Curve shows the accumulative injection charges as a function of the gate voltage (red color). Replotted from Ref. [23].

in PtNs embedded samples under the bias conditions. These peaks are clearly distinguishable from the small oscillations in the background current present at lower gate voltages. A sufficiently larger gate voltage (more than 8 V in this case) is essential to see clear single electron tunneling current due to the microscopic defects in bulk Al_2O_3 or interface states between surrounding Al_2O_3 and PtNs [68]. As the gate voltage becomes more positive, the band bending becomes much larger which significantly decreases the tunneling barrier, and thus electrons can easily tunnel to the PtNs. Thus, SET behavior of PtNs embedded MOS structure was observed at room temperature. When the size of PtNs was decreased from 1.34 to 0.54 nm, the height of the tunneling current was increased. In addition, the average energy separation from neighboring tunneling current peaks closely matches the theoretical calculation of Coulomb charging energy.

ACKNOWLEDGEMENTS

This work was partly supported by the Russian Foundation for Basic Research (Nos. 13-02-12012, 12-02-97029, 12-02-00528) and and by the subsidy allocated to Kazan Federal University for the state assignment in the sphere of scientific activity. A.L. Stepanov is grateful to the Russian Scientific Foundation (No. 14-13-00758).

REFERENCES

[1] A.T. Bell // *Science* **299** (2003) 1688.
[2] A. Cheung, G. de M. Azevedo, C.J. Glover, D.J. Llewellyn, R.G. Elliman, G.J. Foran and M.C. Ridgway // *Appl. Phys. Lett.* **84** (2004) 278.
[3] P.J. Ferreira, O.G.J. Ia, Y. Shao-Horn, D. Morgan, R. Makharia, S. Kocha and H.A. Gasteiger // *J. Electrochem. Soc*. **152** (2005) A2256.
[4] Y. Shao-Horn, W.C. Sheng, S. Chen, P.J. Ferreira, E.F. Holby and D. Morgan // *Top. Catal.* **46** (2007) 285.
[5] M.A. Asoro, D. Kovar, Y. Shao-Horn, L.F. Allard and P.J. Ferreira // Nanotechnol. **21** (2010) 25701-1.
[6] Y.-J. Choi, H.-H. Park, H- Kim. H.-H- Park, H.J. Chang and H. Jeon // *Jap. J. Appl. Phys*. **48** (2009) 35504-1.
[7] T.S. Ahmadi, Z.L.Wang, T.C. Green, A. Henglein and M.A. El-Sayed // *Science* **272** (1996) 1924.
[8] L.D. Rampino and F.F. Nord // *J. Am. Chem. Soc.* **63** (1941) 2745.
[9] A. Henglein, B.G. Ershov and M. Marlow // *J. Phzs. Chem.* **99** (1995) 14129.
[10] D.G. Duff, P.P. Edwards and B.F.G. Johnson // *J. Phys. Chem***. 99** (1995) 15934.
[11] F. Bonet, V. Delmas, S. Grugeon, R. Herrera-Urbina, P.-Y. Silvert and K. Tekaia-Elhsissen // *NanoStruct. Mate*r. **11** (1999) 1277.
[12] A. Goyal, A. Kumar, P.K. Patra, S. Mahendra, S. Tabatabaei, P.J.J. Alvarez, G. John and P.M. Ajayan // *Macromol. Rapid Commun*. **30** (2009) 1116.
[13] 2Q F. Abbasi, H. Mirzadeh and A.A. Katbab // *Polym. Int.* **50** (2001) 1279.
[14] *Metal-Polymer Nanocomposites*, ed. by L. Nicolais and G. Carotenuto (John Wiley & Sons Publ, London, 2004).
[15] B. Karthikeyan, M. Anija and R. Philip // *Appl. Phys. Lett.* **88** (2006) 53104-1.
[16] B. Karthikeyan, M. Anija, P. Venkatesan, C.S. Suchang Sandeep and R. Philip // *Opt. Commun.* **280** (2007) 482.
[17] A. Henglein, B.G. Ershov and M. Malow // *J. Phys. Chem*. **99** (1995) 14129.
[18] L.J. Giovanetti, J.M. Ramallo-Lopez, F.G. Requejo, D.I. Garcia-Gutierrez, M. Jose-Zacaman and A.F. Craievich // *J. Phys. Chem*. C **111** (2007) 7599.
[19] M.J. Yacaman, J.A. Ascencio, H.B. Liu and J. Gardea-Torresdey // *J. Vac. Sci. Technol. B* **19** (2001) 1091.
[20] S. Hazra, A. Gibaud, P. Laffez and C. Sella // *Eur. Phys. J. B* **14** (2000) 363.
[21] M. Yun, D.W. Mueller, M. Hossain, V. Misra and S. Gangopadhyay // *IEEE Electr. Dev. Lett.* **30** (2009) 1362.
[22] R.C. Jeff, M. Yun, B. Ramalingam, B. Lee, V. Misra, G. Triplett and S. Gangopadhyay // *Appl. Phys. Lett.* **99** (2011) 072104-1.
[23] M. Yun, B. Ramalingam and S. Gangopadhyay // *Nanotechnology* **22** (2011) 465201-1.
[24] L.G. Jacobsohn, X. Zhang, A. Misra and M. Nastasi // *J. Vac. Sci. Technol.* **23** (2005) 1470.
[25] P.T. Townsend, P.J. Chandler and L. Zhang, *Optical effects of ion implantation* (Cambridge Univ. Press, Cambridge, 1994).
[26] A.L. Stepanov, D.E. Hole and P.D. Townsend // *Nucl. Instr. Meth. Phys. Res. B* **149** (1999) 89.
[27] A.L. Stepanov In: *Metal-Polymer Nanocomposites*, ed. by L. Nicolais and G. Carotenuto (John Wiley & Sons Publ, London, 2004), p. 241.

[28] A.L. Stepanov. *Ion-synthesis of metal nanoparticles and their optical properties* (Nova Sci. Publ., New York, 2011).
[29] R. Giulian, P. Kluth, B. Johannessen, L.L. Araujo, D.J. Llewellyn, D.J. Cookson and M.C. Ridgway // *Nucl. Instr. Meth. Phys. Res. B* **257** (2007) 33.
[30] A.E. Malik, W.D. Hutchison, N. Nishimura and R.G. Elliman // *Nucl. Instr. Meth. Phys. Res. B* **272** (2012) 70.
[31] R. Giulian, L.L. Araujo, P. Kluth, D.J. Sprouster, C.S. Schnohr, A.P. Byrne and M.C. Ridgway // *J. Phys. D: Appl. Phys*. **44** (2011) 155401-1.
[32] R. Giulian, L.L. Araujo, P. Kluth, D.J. Sprouster, G.J. Foran and M.C. Ridgway // *J. Phys. Condens. Matter* **21** (2009) 155302-1.
[33] R. Giulian, P. Kluth, L.L. Araujo, D.J. Sprouster, A.P. Byrne, D.J. Cookson and M.C. Ridgway // *Phys. Rev. B* **78** (2008) 125413-1.
[34] R. Giulian, P. Kluth, D.J. Sprouster, L.L. Araujo, A.P. Byrne and M.C. Ridgway // *Nucl. Instr. Meth. Phys. Res. B* **266** (2008) 3158.
[35] M.C. Salvadori, F.S. Teixeira, M. Cattani and I.G. Brown // *J. Appl. Phys*. **110** (2011) 114905-1.
[36] S. Nakano, H. Ogiso, H. Sato and S. Nakagawa // *Surf. Coat. Technol*. **128-129** (2000) 71.
[37] S. Nakano, J. Akedo and H. Ogiso // *Surf. Coat. Technol.* **201** (2007) 8539.
[38] F. Mafune, J. Kohno, Y. Takeda, T. Kondow and H. Sawabe // *J. Phys. Chem. B* **104** (2000) 5333.
[39] F. Mafune, J. Kohno, Y. Takeda, T. Kondow and H. Sawabe // *J. Phys. Chem. B* **105** (2001) 5114
[40] F. Mafune, J. Kohno, Y. Takeda and T. Kondow // *J. Phys. Chem. B* **107** (2003) 4218.
[41] U. Kreibig and M. Vollmer, *Optical properties of metal clusters* (Springer, Berlin 1995).
[42] R.C. Johnson, J. Li, J.T. Hupp and G.C. Schatz // *Chem. Phys. Lett*. **356** (2002) 534.
[43] G. Mie // *Ann. Phys.* **25** (1908) 377.
[44] J.A. Creighton and D.G. Eadon // *J. Chem. Soc. Faraday Trans.* **87** (1991) 3881.
[45] P. Chylek // *J. Opt. Soc. Am*. **67** (1977) 561.
[46] W. Mundy, J. Roux and A. Smith // *J. Opt. Soc. Am.* **64** (1974) 1593.
[47] R.E. Benfield, A.P. Maydwell, J.M. van Ruitenbeek and D.A. van Leeuwen // *Y. Phzsik D* **26** (1993) S4.
[48] T. Yonezawa, Y. Gotoh and N. Toshima // *Reactive Polymer* **23** (1994) 43.
[49] N. Toshima and K. Hirakawa // *Appl. Surf. Sci.* **121-122** (1997) 534.
[50] S. Qu, Y. Song, H. Liu, Y. Wang, Y. Gao, S. Liu, X. Zhang, Y. Li and D. Zhu // *Opt. Comm.* **203** (2002) 283.
[51] R.F. Haglund Jr., L. Yang, R.H. Magruder III, J.E. Wittig, K. Becker and R.A. Zuhr // *Opt. Lett.* **18** (1993) 373.
[52] M. Sheik-Bahae, A.A. Said, T.M. Wei, D.J. Hagan and E.W. van Stryand // *IEEE J. Quant. Electron* **26** (1990) 760.
[53] Y. Gao, X. Zhang, Y. Li, H. Liu, Y. Wang, Q. Chang, W. Jiao and Y. Song // *Opt. Commun*. **25**1 (2005) 429.
[54] R.A. Ganeev, A.I. Ryasnyansky, M.K. Kadirov, S.R. Kamalov and T. Usmanov // *J. Phys. D* **34** (2001) 1602.
[55] R.A. Ganeev and A.I. Ryasnyansky // *Appl. Phys. B* **84** (2006) 295.
[56] R.A. Ganeev and T. Usmanov // *Quantum Electronics* **37** (2007) 605.
[57] R.A. Ganeev, M. Suzuki, M. Baba, M. Ichihara and H. Kuroda // *J. Appl. Phys.* **103** (2008) 63102-1.
[58] R.A. Ganeev, R.I. Tugushev and T. Usmanov // *Appl. Phys.* B **94** (2009) 647.
[59] A. Roucoux, J. Schulz and H. Patin // *Chem. Rev.* **102** (2002) 3757.
[60] R. Narayanan and M.A. El-Sayed // *Nano Lett*. **4** (2004) 1343.
[61] V.M. Rudoy, B.G. Ershov, N.L. Sukhov, O.V. Dementeva, A.V. Zaitseva, A.F. Seliverstov, M.E. Kartseva and V.A. Ogarev // *Colloid J.* **64** (2002) 755.
[62] B.G. Ershov // *Izv. Akad. Nauk, Ser. Khim.* **4** (2001) 600.
[63] P.A. Trudinger // *Anal. Biochem*. **36** (1970) 222.
[64] J.T. Lue, W.C. Huang and S.K. Ma // *Phys. Rev. B* **51** (1995) 14570.
[65] K.Y. Cheong, N. Muti S.R. Ramanan // *Thin Solid Films* **410** (2002) 142.
[66] Y.-J. Chou and H.-H. Park // *Thin Solid Films* **519** (2011) 6214.
[67] M.C. Salvadori, M. Cattani, F.S. Teixeira and I.G. Brown // *Appl. Phys. Lett.* **93** (2008) 73102-1.
[68] A. Morales-Sanchez, J. Barreto, C. Dominguez, M. Aceves, Z. Yu and J.A. Luna-Lopez // *Nanotechnol.* **19** (2008) 165401-1.